# Orientation, Hydrogen Bonding, and Penetration of Water at the Organic/Water Interface

**Lawrence F. Scatena and Geraldine L. Richmond***

*Department of Chemistry, University of Oregon, Eugene, Oregon 97403*

*Received: August 18, 2001*

Vibrational sum frequency spectroscopy is used to measure the vibrational spectroscopy of water molecules at the interface between water and several hydrophobic liquids. The studies probe the bonding interactions in the interfacial region between water molecules and molecules in the organic phase. Complementary FTIR and isotopic exchange studies have been used to confirm spectral assignments in the VSF measurements. These studies which largely focus on the $CCl_4/H_2O$ system show that hydrogen bonding interactions weaken and the water coordination number decreases at the interface, relative to the bulk aqueous phase. Although the $CCl_4/H_2O$ system exhibits weak $H_2O-H_2O$ interactions, the interaction of water with the $CCl_4$ phase results in a substantial orientational ordering of these weakly interacting interfacial water molecules. The orientation of these water molecules displays a dependence on the aqueous phase pH, which can be attributed to the screening of the neat interfacial potential, and is displayed through a series of VSF spectroscopic pH experiments. These results are in contrast to the strengthening of hydrogen bonding found for smaller nonpolar solutes in water. The molecular picture emerging from these studies of water structure at hydrophobic liquid surfaces has important relevance to many areas of science including protein folding, membrane structure and function, and the penetration of water into macroscopic structures of a hydrophobic nature.

## Introduction

Water plays a key role in a wide range of molecular and biological processes because of its unique molecular structure and hydrogen bond donating and accepting capabilities. [1] This structure enables water to form an extended hydrogen bonding (H-bonding) network with an extremely high cohesive energy density. Although water makes an excellent solvent for polar molecules, the immiscibility of small nonpolar molecules arises because the stable tetrahedral network of hydrogen bonds in bulk liquid water must be modified in order to solvate small nonpolar solutes.[2] A well developed picture of the environment surrounding a nonpolar solute in an aqueous media has emerged over the past several decades. [3−8] To solvate a small nonpolar entity, water is believed to restructure itself around the solute in such a way as to increase its H-bonding interactions with neighboring water molecules. This results in a reduction in the orientational degrees of freedom allowed to the surrounding water molecules and subsequently leads to an enhancement in the local structure of water around the solute, generally referred to as the iceberg model. [9] This model was initially invoked to account for the anomalously large decrease in entropy that accompanies hydration. This entropy decrease forms the basis of the hydrophobic effect and is believed to play a major role in the important phenomenon known as the hydrophobic-bond, which is the entropy-driven net attraction experienced by pairs of nonpolar solutes in water.

The hydrophobic effect has also been used to explain the structural behavior of large nonpolar macromolecules such as proteins in aqueous solutions. [10−12] Interest in understanding how water interacts with large macromolecules has led to theoretical efforts in modeling the behavior of water adjacent to large extended hydrophobic surfaces, including the air/water,[13−15] hydrophobic-solid/$H_2O$[16] and oil/$H_2O$ interfaces[15,17,18]. The consensus of many of these studies is that as water molecules approach the interface they experience structural changes and an increase in H-bonding interactions with neighboring waters molecules, consistent with the ideas of the hydrophobic effect. This is in contrast to the enthalpy and entropy contributions to the free energy of forming the hydrocarbon/water interface which suggests a decrease in hydrogen bonding when forming such an interface. [19] This raises the question of whether it is appropriate to apply concepts used to describe the hydration of small nonpolar solutes, to larger nonpolar surfaces. This issue has been the topic of numerous insightful theoretical efforts in more recent years. [16,20−23] The strong interest in understanding how hydrophobic hydration varies with the size of the nonpolar surface is driven by a rapidly growing interest in the hydration of biomacromolecules and the clear role of water in their three-dimensional folding and structuring. Whereas there is a wealth of experimental data on water hydration around small solutes, very few experiments have been able to provide a molecular picture of water structure and hydrogen bonding at a large nonpolar liquid surface. This study provides one of the first direct measurements of such water orientation and hydrogen bonding at hydrophobic liquid surfaces.

The primary experimental method employed in these studies is vibrational sum frequency spectroscopy (VSFS). [24−26] Vibrational spectroscopic techniques such as VSFS are valuable for exploring the molecular environment of water at surfaces because the OH vibrational modes of water are very sensitive to different degrees of H-bonding interactions between water molecules. [27−30] The specificity of the second-order VSF process to molecules residing in the asymmetric environment of the interfacial region make it well suited for studies at the liquid/liquid interface. [31] In this paper, we have used VSF spectroscopy to explore the H-bonding interactions of interfacial water at the

* To whom correspondence should be addressed. E-mail: richmond@oregon.uoregon.edu

10.1021/jp0132174 CCC: $20.00 
Published on Web 10/24/2001

$CCl_4/H_2O$ and hydrocarbon/$H_2O$ interfaces and compared these with similar studies of water at the vapor/$H_2O$ interface. To identify interfacial water species contributing to the VSF spectrum, a series of isotopic exchange and FTIR studies have been performed. These studies have allowed the deconvolution of an otherwise broad VSF spectral envelope attained for the interfacial water in the $CCl_4/H_2O$ system into spectral peaks that can be assigned to interfacial water molecules with varying degrees of H-bonding interactions. Overall, we find that water at a hydrophobic liquid interface exhibits weak H-bonding interactions between water molecules relative to the vapor/water interface and other solid/water interfaces previously studied. [32] Instead, weakly attractive interactions between the interfacial water and the organic molecules are a prevalent feature at this interface. These $H_2O$-organic molecular interactions are shown to have a strong orienting effect on weakly interacting interfacial water molecules. The orientation of a portion of these water molecules showing weak interactions can be altered by variations of the aqueous phase pH. These experimental results, which uncover how hydrophobic hydration occurs at hydrophobic liquid surfaces, have important implications for many chemical, technological, and biological processes including the formation of micelles and complex mesostructures in surfactant solutions, the penetration of water into lipids and biomembranes, and the hydration and folding of biopolymers such as proteins and nucleic acids.

**VSFS as an Interfacial Probe.** The physical discontinuity which characterizes interfaces and accounts for the unusual properties of surface molecules, also enables spectroscopic techniques such as VSFS the surface specificity to collect vibrational spectra of interfacial molecules. [33] In general, sum frequency generation, or the coherent coupling of two photons to produce a single photon at the sum of their two frequencies, is described by the absolute square of the second term in the expansion of the macroscopic polarization of a dielectric medium and is proportional to eq 1

$$I(\omega_{SF}) \propto |\chi^{(2)}_{NR} + \sum_{\nu} \chi^{(2)}_{\nu}|^2 I(\omega_{IR}) I(\omega_{vis}) \qquad (1)$$

where $I(\omega_{SF})$ is the intensity of the generated sum frequency, $\chi^{(2)}_{NR}$ and $\sum_{\nu}\chi^{(2)}_{\nu}$ are the nonresonant and resonant second-order nonlinear susceptibility tensors respectively, which describe the nonlinear response of the medium to the intensity of the two radiation fields $I(\omega_{IR})$ and $I(\omega_{vis})$. The nonresonant contribution varies little with frequency and is small for systems studied using nanosecond pulsed lasers that have inherently low peak intensities (relative to their pico- and femtosecond counterparts) and systems with relatively low polarizabilities such as the liquid/liquid systems described herein.

The molecular specificity of this spectroscopic technique is best described by the resonant contribution ($\chi^{(2)}_{\nu}$) given in eq 2

$$\chi^{(2)}_{\nu} \propto \frac{A_{\nu}}{\omega_{IR} - \omega_{\nu} + i\Gamma_{\nu}} \qquad (2)$$

which is summed over all SF active vibrational modes of interfacial molecules and is the dominant contribution to the detected VSF intensity. The terms $\omega_{IR}$ and $\omega_{\nu}$ correspond to the frequencies of the IR radiation and molecular vibrational transition respectively, $\Gamma$ is the natural line width of the transition, and $A_{\nu}$ is the amplitude coefficient proportional to the product of the Raman and IR transition moments. In a VSFS experiment, the sum frequency "transition probability" becomes the absolute square of the second-order nonlinear susceptibility tensor ($\chi^{(2)}$). Therefore, to be SF active, molecules must have vibrations with nonzero IR and Raman cross sections and be located within a molecular environment that lacks an inversion center (e.g., at an interface).

In addition to measuring the vibrational spectra of interfacial species, VSFS experiments can be used to ascertain the orientation of molecular species with the judicious choice of polarizations for SF, visible, and IR radiation, which access different components of the $\chi^{(2)}$ tensor. Experiments described herein have been performed mainly by collecting SF radiation under *s,s,p* polarization conditions, which refer to the polarizations of SF, vis, and IR radiation, respectively. Under $I_{s,s,p}$ polarization conditions, experiments access vibrational modes with a component of their transition dipole normal to the interfacial plane. [33] $I_{s,p,s}$ and $I_{p,s,s}$ measure the in-plane response.

Relative to vibrational spectroscopic methods such as IR absorption or Raman spectroscopy, the coherent nature VSF spectroscopy requires a more complex spectral analysis procedure to deconvolute overlapping vibrational bands. [33−36] In second-order nonlinear spectroscopic techniques such as VSFS each vibrational band has an inherent phase for a fixed molecular orientation and variation of phase occurs with a change in orientation. [25,37] It is the overlapping of vibrational modes of opposite or congruent phases which contributes to destructive and constructive interferences that lead to the asymmetric character of overlapping vibrational bands in the VSF spectrum.[38] Typically, to account for phase relationships between individual vibrational peaks a Lorentzian distribution of vibrational energies is assumed and each vibrational transition is represented by eq 2. The problem with using the Lorentzian line shape is that it is typically used to model homogeneously broadened transitions, and it also over estimates the amount of overlap and therefore interference between widely separated peaks. In an attempt to realistically model the inhomogeneously broadened vibrational transitions of liquid phase water and interferences between adjacent vibrational bands, our fitting routine employs a line shape similar to a Voigt profile. This line shape expression is a convolution of eq 2, which accounts for homogeneous broadening, and a Gaussian distribution. Despite being computationally more intensive, this convolution of line shapes more accurately models the distribution of molecular environments and supplies each vibrational mode with a phase factor therefore modeling the coherent nature of the nonlinear technique. Although the accompaniment of a phase factor with each vibrational mode complicates spectral analysis, accurate spectral fits not only render differing interfacial H-bonding environments in the case of $H_2O$ but also the added benefit of molecular orientation. A detailed description of the spectral fitting method is beyond the scope of this article but is the focus of an earlier paper by Brown et al. [37]

In a typical VSF experiment, a tunable infrared laser source ($\omega_{IR}$), which is varied across the vibrational energy region of molecules of interest, and a fixed frequency visible laser source ($\omega_{vis}$) are incident both temporally and spatially on the surface. The generated SF ($\omega_{SF} = \omega_{vis} + \omega_{IR}$) radiation is collected and corresponds to the absolute square of the resonant term ($\chi^{(2)}_{\nu}$). When the collected SF radiation is plotted against the IR energy the result is a vibrational spectrum of molecules located in the interfacial region. In accordance with VSFS selection rules, molecules residing within the centrosymmetric bulk environment will not give rise to SF signal. Hence, VSFS is a powerful spectroscopic technique for separating molecularly specific spectroscopic contributions from bulk and interfacial molecules.

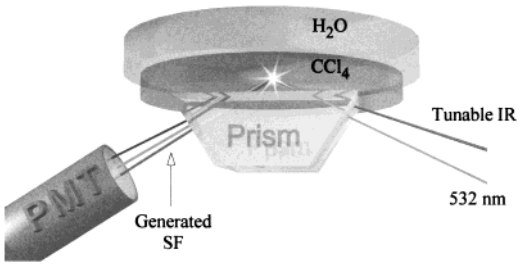


**Figure 1.** Diagram of VSF experimental setup for the $CCl_4/H_2O$ system. VSF spectra are collected such that both IR and 532 nm pass through an IR grade quartz prism and a ~2 mm path length of $CCl_4$ where they are totally internally reflected at the $CCl_4/H_2O$ interface. The generated SF beam is collected using wavelength discriminating optics, photomultiplier tube and gated electronics.

## Experimental Section

The laser system employed for the VSF experiments performed at the $CCl_4/H_2O$ and hexane/$H_2O$ interfaces consists of a Nd:YAG (Coherent, Infinity-100) diode seeded pump laser with the fundamental output of 1064 nm. The 20 Hz repetition rate pump laser generates ~4 nanosecond pulses with 500 mJ/pulse in a beam area of 0.24 $cm^2$, thus producing peak intensities of 477 MW/$cm^2$. These peak intensities allow generation of coherent visible and mid-infrared light by parametric generation and difference frequency mixing in a double pass optical parametric oscillator/optical parametric amplifier (DPOPO/OPA) in series. The fundamental of the pump laser is split into two segments and 60 mJ of the 1064 nm beam is frequency doubled in a BBO crystal to provide 532 nm light for use at the experiment, whereas the second segment is directed into the DPOPO/OPA. The portion of 1064 nm fundamental sent into the DPOPO/OPA is split into two segments. The first segment is frequency doubled using a KTP crystal to provide 532 nm pump light for the DPOPO. The DPOPO contains two angle tuned KTP nonlinear crystals phasematched under type II phasematching conditions. Signal (746−840 nm) and idler (1.85−1.44 nm) photons are produced by parametric generation within the nonlinear crystals and the wavelengths are varied by angle tuning the crystals in the plane of the laser table. Due to the short pulse length of the pump laser the output coupler of the DPOPO is highly reflective at 532 nm thus allowing the pump pulse to take a second pass through the cavity before exiting. The idler portion of the DPOPO is then combined and propagated collinear with the second segment of the 1064 nm pump beam in the OPA. The OPA contains two angle tuned (within the plane of the table) type II phasematched KTA nonlinear crystals. Within the OPA mid-infrared light is generated by the nonlinear process of difference frequency mixing. Filtering optics are used to descriminate 1.064 nm, 532 nm, and signal (1.85−1.44 nm) radiation from the mid-IR radiation to be used at the experiment. The frequency of the coherent mid-infrared radiation is varied by computer control and tunable from 2.5 to 4 $\mu$m with energies of approximately 2 mJ at 2.5 $\mu$m to 1 mJ at 4 $\mu$m and has a bandwidth near 1 $cm^{-1}$. Nearly 90% of the IR path length is contained within an atmosphere that is circulated over activated charcoal and anhydrous calcium sulfate to remove atmospheric water vapor. IR adsorptions by rovibrational bands of residual water vapor are responsible for sharp (1−4 $cm^{-1}$ fwhm) intensity dips in SF spectra between 3550 and 3800 $cm^{-1}$.

The $CCl_4/H_2O$ experiments have been performed using a Kel-F cylindrical cell that is place on top of an IR grade quartz prism (Figure 1). Doubly distilled $CCl_4$ (Aldrich, 99.9% HPLC grade) was placed in the cell and covered with $H_2O$ (Mallinckrodt ChromAR HPLC Grade). The collimated (~1 mm) 532 nm radiation is coupled into the cell through the prism at its critical angle (66° to the surface normal) where it enters into the Kel-F cell through an aperture at the base. As the 532 nm radiation passes from the high index of refraction medium ($CCl_4$: $n^{20} = 1.4607$) to the low index medium ($H_2O$: $n^{20} = 1.3330$) it is totally internally reflected (TIR) at the $CCl_4/H_2O$ interface. [39] Under these conditions sum frequency signal is enhanced by several orders of magnitude over an externally reflected geometry. [40,41] The TIR geometry allows the detection of low SF water signal levels associated with the nanosecond pulse length radiation relative to pico or femtosecond pulses. The IR radiation is coupled into the cell at an angle of ~73° to the surface normal in a copropagating configuration. The IR beam diameter incident on the interface was approximately 500 $\mu$m. The thickness of the $CCl_4$ layer and angle of IR incidence were adjusted such that the IR path length is reduced to ~1−2 mm in order to reduce IR absorption by monomeric $H_2O$ within the $CCl_4$ phase. The 532 nm and IR radiation are overlapped spatially and temporally at the $CCl_4/H_2O$ interface and the SF radiation collected on reflection at an angle defined by conservation of momentum. Although spatially separated, the 532 nm and SF radiation are further separated using a combination of absorptive, interference and holographic notch filters. A Glann−Taylor broad band polarizer is used prior to SF collection to select the desired SF polarization. The SF radiation is collected using a PMT, gated electronics, and computer. Each VSF $CCl_4/H_2O$ spectrum is obtained with an increment of 2 $cm^{-1}$ and an average of 50−100 pulses per increment. The VSF spectrum of the hexane/$H_2O$ interface has been taken in a TIR geometry, in a manner similar to the $CCl_4/H_2O$ system.

The vapor/$H_2O$ VFS spectrum has been taken with a 2 ps laser system overlapping 275 $\mu$J of 800 nm and 3−13 $\mu$J of 2700−4000 $cm^{-1}$ radiation on the interface in an external reflection geometry. [42,43] The vapor/$H_2O$ (Mallinckrodt ChromAR HPLC Grade $H_2O$) experiments were performed in a $N_2$ purged closed cell such that contamination of the interface is minimized.

FTIR isotopic exchange studies in bulk $CCl_4$ have been performed in a 1 cm path length IR grade quartz cell at 295 K. $D_2O$ (Cambridge Isotope Laboratories, 99.996%, used in both FTIR and VSF experiments) was shaken over doubly distilled $CCl_4$ (Aldrich, 99.9% HPLC grade) which produces HOD by isotopic exchange with trace amounts of $H_2O$. HCl (Fisher Scientific) and NaOH (Fisher Scientific) solutions have been used to adjust the pH of the aqueous phase. All glassware and experimental apparatus that came in contact with aqueous phases have been soaked in concentrated sulfuric acid containing Nochromix to remove any organics and surface-active contaminants. After removal from concentrated acid, equipment has been thoroughly rinsed with 17.9 MΩ water from a Nanopure filtration system until free from acid residue.

## Results and Discussion

The VSF spectrum of water measured at the vapor/$H_2O$, $CCl_4/H_2O$, and hexane/$H_2O$ interfaces are shown in Figure 2a-c, respectively. The measurements are taken in the spectral region of the OH stretching modes of water. The spectrum for the vapor/$H_2O$ interface is distinctly different from that of the liquid/liquid interfaces, indicative of a difference in the H-bonding interactions between interfacial molecules at the vapor/$H_2O$ and organic/$H_2O$ liquid interfaces. Our most extensive work has been performed on the $CCl_4/H_2O$ system and will be the focus of much of this study. The hexane/$H_2O$ studies are provided as an

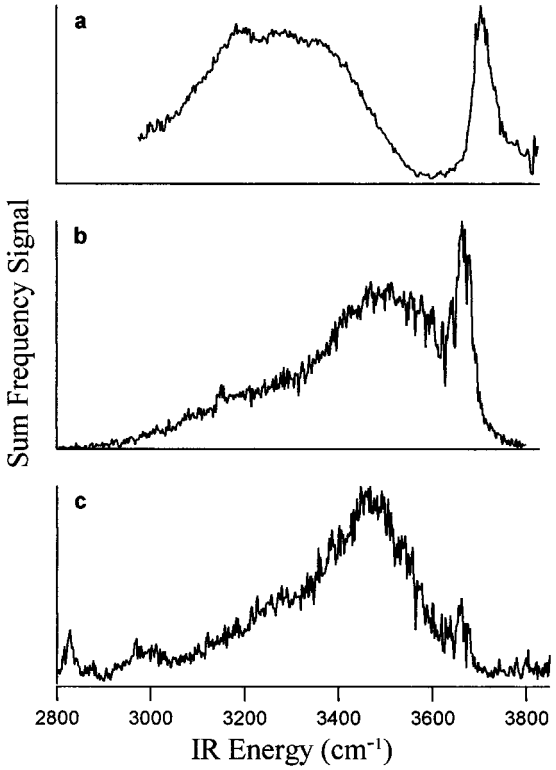


**Figure 2.** VSF spectra of the vapor/$H_2O$ **(a)**, $CCl_4/H_2O$ **(b)**, and hexane/$H_2O$ interfaces **(c)**, indicating the differences in H-bonding environments at the various interfaces.

example of the generality of the observations made in the $CCl_4/H_2O$ system [44] and will be covered in great detail in a forthcoming publication. [45]

The interpretation of spectral features displayed in these two spectra requires a discussion of the vibrational signatures for different types of $H_2O$ bonding interactions. IR and Raman vibrational spectroscopic studies have been used extensively to assign specific spectral features in the 3100−3800 $cm^{-1}$ region to the various types of water species and structures present in bulk phase water. The OH stretching ($\nu_1$ & $\nu_3$) region of water extends from near 3100 $cm^{-1}$ to 3800 $cm^{-1}$ and is strongly dependent on the strength of H-bonding interactions between water molecules. [1,46,47] In its vapor phase, water largely exists in its monomeric form where both hydrogens are equivalent and therefore energetically couple. The coupling gives rise to the localized symmetric ($\nu_1$) and asymmetric stretching modes ($\nu_3$) which occur at 3657 and 3756 $cm^{-1}$, respectively, for water monomers. [47] As water condenses into its liquid phase, the altered molecular environment is characterized by red shifted OH stretching frequencies due to increased H-bonding interactions and weakening of OH oscillator strength. [1,47] The increased $H_2O-H_2O$ interactions also tend to broaden spectral features and complicate spectral interpretation due to the overlap of broad H-bonded $\nu_1$ and $\nu_3$ bands in the 3200−3400 region of the spectra. Consequently, spectral interpretation in the ∼3100−3400 $cm^{-1}$ region has been the most challenging due to the broad spectral features associated with water molecules participating in multiple hydrogen bonds. Intimately coupled to the greater H-bonding interactions between water molecules, the dipole transition moment of these modes also increase as manifested in an increase in the integrated band intensity with the corresponding red shift in stretching frequencies. [47] The onset of nucleation with the transformation of liquid water into ice produces a shift further into the red as H-bonding interactions become even stronger. The increased $H_2O-H_2O$ interactions and enhanced intermolecular coupling of water in its solid form appear as sharp spectral features in the 3100−3200 $cm^{-1}$ region.[1,47−52]

VSF spectra of interfacial water species contain many of the same spectral features of the IR and Raman studies that can be associated with vapor, liquid, and ice phases of water. The main contribution to the OH stretching region for vapor/$H_2O$ studies has been attributed to the $\nu_1$ mode [27,29,53] due to the low Raman transition probability of the $\nu_3$ stretching mode. [32,47] The 3200 $cm^{-1}$ region has typically been assigned to intermolecularlly coupled $\nu_1$ of symmetrically bonded ($\nu_1$(SB)), tetrahedrally coordinated water molecules participating in extensive H-bonding. This assignment originates from comparison of Raman and IR spectra of ice and supercooled liquid water [47,49,50,54−56] and suggests that the features in the 3200 $cm^{-1}$ region are indicative of water in a more ice type H-bonding environment. Similar comparisons of Raman and IR spectra of liquid water[49,50,54] have lead to the assignment of spectral features in the 3400 $cm^{-1}$ region. These have been assigned to $\nu_1$ of tetrahedrally coordinated, asymmetrically bonded water molecules with a more random molecular arrangement. VSF spectral bands which appear in the 3200−3400 $cm^{-1}$ region have therefore been termed "ice-like" (3200 $cm^{-1}$) and "liquid-like" (3400 $cm^{-1}$) $\nu_1$ modes of water due to their similarity in spectral position and widths with their respective bulk bands in IR and Raman experiments.

VSF spectra of the vapor/$H_2O$ system, shown here (Figure 2a) and in other studies, [28,53,57] exhibit intensity in both the 3200 and 3400 $cm^{-1}$ regions, suggesting interfacial water is participating in both strong symmetric and weaker asymmetric type H-bonding interactions. A sharp spectral feature located near 3700 $cm^{-1}$ is also observed in the vapor/$H_2O$ spectrum. This region is characteristic of water molecules with minimal $H_2O-H_2O$ interactions. The 3700 $cm^{-1}$ peak corresponds to the free OH bond of water molecules that straddle the interface. [53] This bond, which is directed into the vapor phase, is energetically uncoupled from the adjacent intramolecular OH bond that does participate in H-bonding with neighboring water molecules. This situation leads to two distinct intramolecularly uncoupled OH stretching modes, which analogous to gas-phase vibrational spectra of water dimers, gives rise to a free and bonded OH stretch of the H-bond donating water molecule. [58,59] This intramolecularly uncoupled and unperturbed OH oscillator at 3700 $cm^{-1}$ (Figure 2a) is located directly between the coupled $\nu_1$ (3657 $cm^{-1}$) and $\nu_3$ (3756 $cm^{-1}$) modes of monomeric vapor water, as governed by the linear superposition of states. The location of the uncoupled bonded OH stretching mode of these water molecules that straddle the interface have not been addressed in previous VSF water studies.

For the $CCl_4/H_2O$ (Figure 2b) interface, spectral features in the region of weakly interacting water molecules dominate the VSF spectrum relative to the vapor interface. The two most prominent bands occur in the 3500−3700 $cm^{-1}$ region, where water molecules with weak H-bonding interactions occur. The $CCl_4/H_2O$ system also lacks significant spectral intensity in the 3200 $cm^{-1}$ region, an indication that there is little contribution from water molecules participating in strong tetrahedrally coordinated H-bonding interactions. A qualitative comparison of the spectral contours of the two systems (vapor/$H_2O$ and $CCl_4/H_2O$) indicates that the $CCl_4/H_2O$ interfacial environment largely contains water molecules participating in weak hydrogen interactions. In contrast, the vapor/$H_2O$ interface exhibits strong

intensity in the 3200 $cm^{-1}$ region and lack of intensity in the 3500−3700 $cm^{-1}$ region indicating stronger H-bonding interactions.

Spectral features that indicate weak H-bonding interactions (3500−3700 $cm^{-1}$) are not unique to only the $CCl_4/H_2O$ system but have been recently observed at hexane/$H_2O$ (Figure 2c) and hexene/$H_2O$ surfaces [44] and suggest that these liquid/liquid systems have similar interfacial water environments. Spectral interpretation in the 2800−3200 $cm^{-1}$ region of the alkane/$H_2O$ systems is complicated by the fact that CH stretching modes absorb incident IR radiation in this spectral region and can complicate the interpretation. For the data in Figure 2c, a thin layer of hexane was employed to minimize adsorption of the incident IR beam. The $CCl_4/H_2O$ system is void of this complication. Hence, this system allows us to take a more detailed analytical look at the interfacial water environments which contribute to the VSF spectrum of the neat $CCl_4/H_2O$ interface and how this interfacial water structure compare with water at other surfaces and theoretical calculations.

When experimental results for the $CCl_4/H_2O$ and alkane/$H_2O$[44] systems described herein are compared with similar studies of the $CCl_4/H_2O$ interface by Gragson et al. [60] and the hexane/$H_2O$ interface by Du et al. [27] one notices an obvious discrepancy in spectral intensity in the 3200 $cm^{-1}$ and 3500−3600 $cm^{-1}$ regions of the VSF spectra. These earlier studies exhibit little spectral intensity in the 3500−3600 $cm^{-1}$ region and large intensities in the 3200 $cm^{-1}$ region. This was interpreted as an enhancement of the water structure at these surfaces. In contrast, recent VSF studies by our group at both $CCl_4/H_2O$ and alkane/$H_2O$ interfaces indicate that there is significant intensity in these regions. Over the course of extensive experiments in our lab involving the $CCl_4/H_2O$ interface, it has become clear that the structure and H-bonding of interfacial water molecules are *highly* sensitive to trace amounts of impurities that tend to concentrate at the interface. As the impurities are progressively removed spectral features in the 3400−3600 $cm^{-1}$ region grow in and spectral intensity in the 3200 $cm^{-1}$ region diminishes resulting in the VSF spectrum in Figure 2b. Similar changes have been observed at several alkane/$H_2O$ interfaces. [44] These finding have therefore modified previous interpretations, and can readily account for the differences between our observations and previous $CCl_4/H_2O$ [60] and hexane/$H_2O$ [27] VSF studies.

**Isotopic Dilution Measurements.** In an effort to separate the VSF $CCl_4/H_2O$ spectral envelope into discrete $H_2O$ spectral bands, corresponding to water molecules in distinct interfacial H-bonding environments, FTIR and VSF isotopic exchange studies have been performed. The IR spectrum of a dilute solution of HOD in $CCl_4$ is shown in Figure 3a and corresponds to the OH vibrational spectrum of monomeric HOD. By exchanging one hydrogen atom with a deuterium atom, the ensuing HOD molecule contains two oscillators with different vibrational energies. These oscillators are energetically uncoupled, similar to water molecules that straddle the vapor/$H_2O$ interface where one hydrogen is bonding with the aqueous phase (bonded OH) and the other interacting with the vapor phase (dangling or free OH). Only one spectral feature at 3663 $cm^{-1}$ is present in the OH stretching region. This feature is assigned to the free OH stretch of an energetically uncoupled monomeric HOD molecule where both hydrogen and deuterium are interacting with the $CCl_4$ solvent. Similar IR isotopic exchange experiments previously performed in bulk $CCl_4$ observe the OH oscillator at similar peak frequencies. [61−64]

The results of related VSF isotopic exchange experiments at the $CCl_4/H_2O$ interface are displayed in Figure 3b. Surface

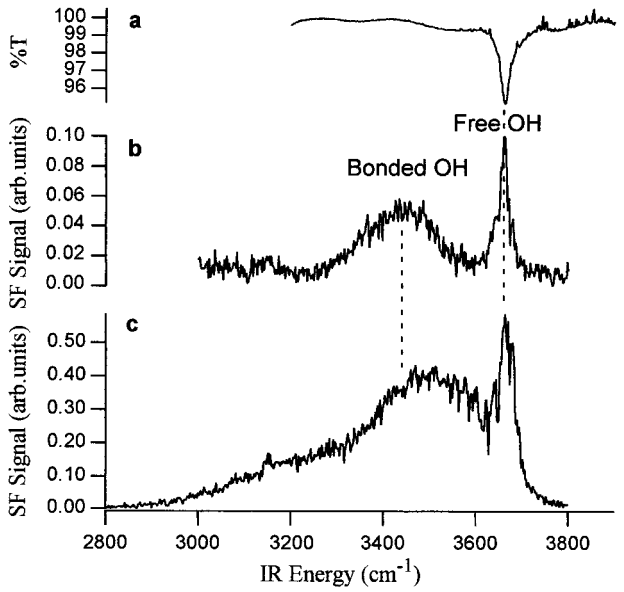


**Figure 3.** Comparison of the VSF isotopic exchange studies at the $CCl_4$/water interface and in bulk $CCl_4$ with the VFS spectrum of the neat $CCl_4/H_2O$ interface. **a.** FTIR spectrum of trace amounts of monomeric HOD in bulk $CCl_4$. Spectral feature located at 3663 $cm^{-1}$ corresponds to the uncoupled free OH oscillator of monomeric HOD. **b.** VSF spectrum of HOD at the $CCl_4$/water interface. At mole fractions of 0.198 and 0.012 for HOD and $H_2O$ respectively, SF signal in the OH stretching region originates primarily from HOD molecules. Spectral features located at 3438 and 3667 $cm^{-1}$ correspond to the uncoupled bonded and free OH oscillator of interfacial HOD, respectively. **c.** VSF spectra of neat $CCl_4/H_2O$ interface for spectral comparison.

isotopic experiments such as this reduce intra and intermolecular coupling that tends to broaden spectral features in the case of $H_2O$, [64−69] The VSF spectrum of interfacial HOD at the $CCl_4$/water interface exhibits a sharp feature located near 3667 $cm^{-1}$ and a broad feature near 3438 $cm^{-1}$. Under dilute concentrations of HOD in $D_2O$, as performed in this experiment, the VSF spectrum should contain only two spectral features in the OH stretching region as observed here. The spectral feature located at 3667 $cm^{-1}$ corresponds to the OH bond of interfacial HOD molecules that are interacting with the $CCl_4$ phase. This type of HOD molecule will give rise to a localized OH stretching mode near what is observed in Figure 3a and therefore the peak at 3667 $cm^{-1}$ is assigned to the free OH oscillator. We assign the second broad spectral feature to the OH bond of interfacial HOD molecules that are participating in H-bonding interactions with the aqueous phase. Contribution to this spectral feature will include two types of interfacial HOD molecules: (1) HOD molecules that straddle the interface with the OH oscillator directed toward and interacting with the aqueous phase or (2) interfacial HOD molecules that have both OH and OD bonds interacting with the aqueous phase. The inhomogeneous H-bonding environments experienced by an uncoupled bonded OH mode leads to the broadened spectral feature at 3438 $cm^{-1}$ as compared to the sharp free OH oscillator mode. Assignment of the uncoupled bonded OH oscillator is also consistent with earlier Raman and IR experiments that indicate spectral features in the region of 3400−3460 $cm^{-1}$ originate from the OH oscillator of H-bonded HOD molecules in liquid water. [49,64,67,69,70] We observe a similar peak in this region when VSF HOD experiments are conducted at the vapor/$H_2O$ interface, which we attribute to similar uncoupled bonded water species. [71]

Figure 3c contains the VSF spectrum of the neat $CCl_4/H_2O$ interface for comparison with FTIR (Figure 3a) and VSF (Figure

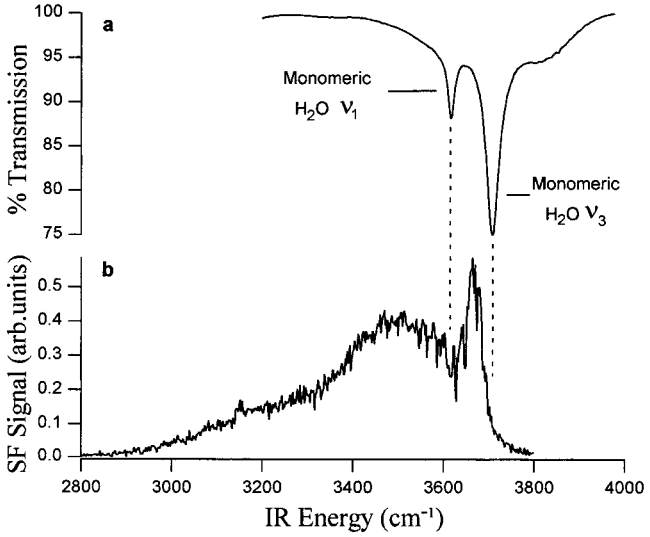


**Figure 4.** Comparison of the vibrational spectrum of monomeric water in bulk $CCl_4$ to the neat $CCl_4/H_2O$ VSF spectrum. **a.** FTIR spectrum of trace amounts of $H_2O$ dissolved in $CCl_4$. The spectral features located at 3616 and 3708 $cm^{-1}$ correspond to $\nu_1$ and $\nu_3$ normal modes respectively, of monomeric $H_2O$ in bulk $CCl_4$. Vertical axis is in percent transmittance (%T). **b.** VSF spectra of neat $CCl_4/H_2O$ interface for spectral comparison.

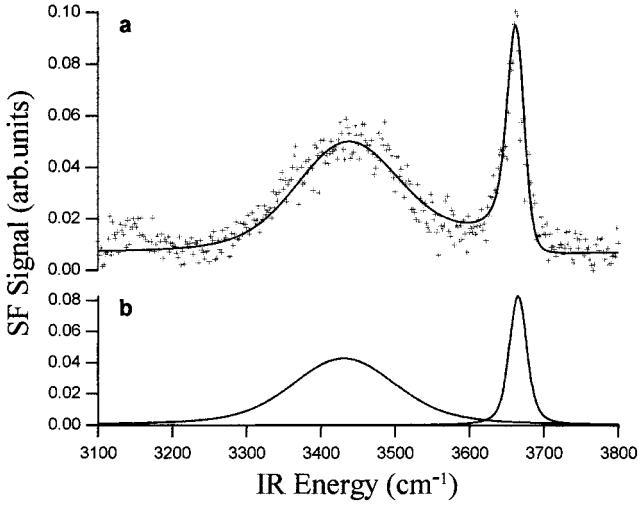


**Figure 5.** Spectral fit to the interfacial isotopic exchange data. **a.** VSF spectrum of HOD at the $CCl_4$/water interface with the nonlinear least squares spectral fit to the data superimposed as a solid line. Peak parameters are displayed in Table 1. **b.** Peak positions for the various OH modes derived from the fit to the data in Figure 5a.

3b) isotopic experiments performed in bulk $CCl_4$ and at the $CCl_4$/water interface, respectively. Comparison of spectral position and width of the bonded uncoupled OH stretching mode (Figure 3b) with the spectral envelope in Figure 3c indicates that considerable spectral intensity in the 3440 $cm^{-1}$ region originates from the uncoupled bonded OH oscillator. In addition the spectral position of the free OH oscillator in Figure 3a,b coincides well with the sharp spectral feature at 3669 $cm^{-1}$ in the spectrum of the neat $CCl_4/H_2O$ interface. The remaining spectral intensity below 3400 $cm^{-1}$ is attributed to intramolecularly coupled modes of interfacial water. This is consistent with the fact that VSF intensity in the 3200 $cm^{-1}$ region (Figure 3c) is attributed to the $\nu_1$ mode (coupled mode) of tetrahedrally coordinated $H_2O$ and that this region lacks significant intensity in the VSF spectrum of interfacial HOD (Figure 3b).

The lack of spectral bands in the 3600 $cm^{-1}$ region of the VSF HOD spectrum and significant intensity in this region in the VSF spectrum of the $CCl_4/H_2O$ interface, prompted the spectroscopic investigation of monomeric $H_2O$ in $CCl_4$. Molecules that interact solely with $CCl_4$ would be expected to have modes near the 3600 $cm^{-1}$ region as a result of weak $CCl_4-H_2O$ interacions. Water solvated by $CCl_4$ has been the focus of many spectroscopic studies [47,64,72−74] aimed at understanding the influence of solute−solvent interactions on the infrared spectra of water in nonpolar solvents. Figure 4a is the IR spectrum taken in our laboratory of water monomers in $CCl_4$ (mole fraction $_{(H2O)} < 10^{-4}$). [64] The infrared spectrum gives rise to two well-defined peaks corresponding to the $\nu_1$ (symmetric, 3616 $cm^{-1}$) and $\nu_3$ (asymmetric, 3708 $cm^{-1}$) OH stretching modes of an isolated water molecule and agrees with previous work. [72,74] The small red shift of these two stretching modes, as compared to their vapor phase counterparts ($\nu_1$: 3656.7, $\nu_3$: 3755.8), [47] reflects the solvent−solute interactions and the low dielectric constant of the $CCl_4$ phase. More detailed studies by Conrad et al. [74] have shown that the peak frequency, intensity, and width of both $\nu_1$ and $\nu_3$ modes are very sensitive to interactions with the organic phase. From the comparison between the IR spectrum of monomeric $H_2O$ in $CCl_4$ (Figure 4a) with the VSF spectra of water at the neat $CCl_4/H_2O$ interface (Figure 4b) we conclude that intensity in the 3600 $cm^{-1}$ and to a lesser extent 3700 $cm^{-1}$ region of the neat $CCl_4/H_2O$ spectrum is due to monomeric $H_2O$ in the interfacial region. Results of the VSF isotopic exchange study (Figure 3b) also concur with this interpretation given the lack of intensity in the 3616 and 3708 $cm^{-1}$ regions, indicating that intensity in these regions originate from the intramolecularly coupled modes of $H_2O$. Spectral intensity in this region for the hexane/$H_2O$ spectrum indicates that these weakly interacting water molecules are also present in that system. [74]

**Spectral Assignments and Orientational Information.** To assist in the assignment of spectral features in the $CCl_4/H_2O$ spectrum to different types of interfacial water interactions, information such as spectral position and width of the various H-bonding environments of water were taken from the series of isotopic exchange (Figure 3a,b) and dilute $H_2O$ in bulk $CCl_4$ (Figure 4a) experimental results described above. This information was used as input into the calculation of the overall fit to the data in Figure 2b. Figure 5a displays the nonlinear least-squares fit to the VSF spectrum of HOD at the $CCl_4$/water interface. Parameters derived from the spectral fit are summarized in Table 1. As shown in Figure 5a, an excellent fit to the data is obtained using the experimental input. For these and later fits, the relative phase of the peaks was derived from the fits, providing informantion of the relative orientation of contributing modes. Analysis of the VSF isotopic exchange results indicate that the peaks corresponding to the uncoupled free OH oscillator located at 3667 ± 1 $cm^{-1}$ and the uncoupled bonded OH oscillator located at 3438 ± 2 $cm^{-1}$ are fit with positive and negative phases (amplitudes) respectively, an indication that these two modes are near 180° out of phase. The assignment of positive amplitude for the free OH oscillator corresponds to an average orientation of the dipole vector, defined as pointing from electropositive to electronegative, pointing toward the aqueous phase or $\theta < 90°$ (hydrogen atom directed into the $CCl_4$ phase). Where $\theta$ refers to the Euler angle between the symmetry axis of the uncoupled OH oscillator and the $Z$ axis, (laboratory frame) which points away from the $H_2O$ phase and normal to the interfacial plane. This orientation is in complete accordance with molecular dynamics simulations of the $CCl_4/H_2O$ interface [17] that also suggest that OH oscillators not participating in H-bonding are on average oriented perpen-

**TABLE 1: Results from the Nonlinear Least-squares Fit to the Data Collected for HOD at the $CCl_4$/Water Interface (Figure 5a) and $H_2O$ at the Neat $CCl_4/H_2O$ Interface (Figure 6a)[a]**

| | frequency ($\omega_\nu$/cm$^{-1}$) | width ($\Gamma_\nu$/cm$^{-1}$) | amplitude ($A_\nu$) | orientation |
|---|---|---|---|---|
| | interfacial $H_2O$ | | | |
| $\nu_1$ symmetrically bonded | 3247 | 284 | −0.34 | $\theta > 90°$ |
| uncoupled bonded OH | 3439 | 226 | −0.51 | $\theta > 90°$ |
| undetermined | 3570 | 62 | 0.07 | $\theta < 90°$ |
| $\nu_1$ monomeric/HB acceptor | 3617 | 66 | 0.29 | $\theta < 90°$ |
| uncoupled free OH | 3669 | 46 | 0.85 | $\theta < 90°$ |
| $\nu_3$ monomeric/HB acceptor | 3716 | 66 | −0.26 | $\theta > 90°$ |
| | interfacial HOD | | | |
| uncoupled bonded OH | 3441 | 164 | −0.21 | $\theta > 90°$ |
| uncoupled free OH | 3665 | 26 | 0.34 | $\theta < 90°$ |

[a] The phase (amplitude) of the free OH vibration is assigned a positive value consistent with the dipole orientation pointing toward the aqueous phase. The positive/negative sign associated with each amplitude parameter reflects the phase of a particular molecular vibration. Small adjustments to individual parameters can give rise to satisfactory fits; however, the signs of the amplitudes and, hence, the orientational information, were consistent through rigorous testing of other possibilities. Improvements in the fitting method have made small changes to fit parameters, as compared to those previously published.[37,44]

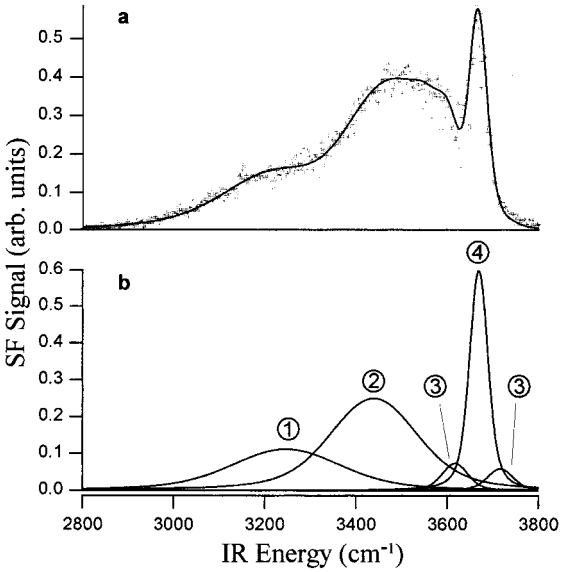


**Figure 6.** Spectral fit to VSF spectrum of the neat $CCl_4/H_2O$ interface. **a.** VSF Spectrum of the neat $CCl_4/H_2O$ interface with the nonlinear least squares spectral fit to the data superimposed as a solid line. Peak parameters are displayed in Table 1. **b.** Peak positions for the various OH modes derived from the fit to the data in Figure 6a. Each contributing peak is labeled with a number, which corresponds to a specific interfacial $H_2O$ species that is displayed in Figure 8.

dicular to the interfacial plane with the hydrogen directed toward the $CCl_4$ phase. Relative to the free OH oscillator, the uncoupled bonded OH oscillator is found to have negative amplitude, an indication that the uncoupled free and bonded OH modes are approaching a 180° phase relationship. This phase relationship signifies that the average orientation of the bonded OH oscillator is with its dipole vector pointing toward the $CCl_4O$ phase where the proton participates in H-bonding.

Figure 6a displays the nonlinear least-squares fit to the neat $CCl_4/H_2O$ VFS spectrum and parameters derived from the spectral fit are summarized in Table 1. As shown in Figure 6a, the spectral fit to the data is excellent using the input derived from the FTIR and isotopic VSF experiments described above. There are three main contributors to the neat $CCl_4/H_2O$ spectral envelope. The most prominent fitted spectral feature is located at 3669 ± 1 cm$^{-1}$ and corresponds to the uncoupled free OH oscillator. The spectral position and width or this peak correlate well with the uncoupled free OH oscillator of HOD experiments (Figure 3a,b) performed by this lab and those by Downey et al.[61] (3664 cm$^{-1}$) and Zoidis et al. [64] (3663 cm$^{-1}$) in bulk $CCl_4$. The narrow width of this peak and close spectral proximity to the dangling or free OH band in the vapor/$H_2O$ studies support this assignment. This further supports the conclusion that the peak at 3669 cm$^{-1}$ arises from an interfacial water molecule with one of its hydrogens interacting with the $CCl_4$ phase (free OH), whereas the other hydrogen protrudes into the aqueous phase. The red shift in the free OH oscillator's peak position relative to its vapor/$H_2O$ position reflects the interaction of the hydrogen with the $CCl_4$ phase. The calculated binding energy for the $H_2O-CCl_4$ dimer is reported to be −1.4 kcal/mol. [17] Previous experimental results and theoretical calculations involving the interaction of water with nonpolar solvents such as $CCl_4$ are in complete accordance with these results. [17,72,74]

The fitted spectral peak located at 3439 ± 5 cm$^{-1}$ is assigned to the adjoining uncoupled bonded OH oscillator due to its broad spectral width, equivalent interfacial HOD spectral position (Figure 3b, 3438 cm$^{-1}$) and numerous literature values[49,64,67,69,70,75] that place the uncoupled bonded OH oscillator between 3400 and 3500 cm$^{-1}$. Because this mode has spectral intensity comparable to the free OH, this indicates that the uncoupled bonded OH mode is oriented such that it has a significant dipole component perpendicular to the interfacial plane. The positive and negative amplitudes associated with the free (3669 cm$^{-1}$) and bonded (3439 cm$^{-1}$) OH oscillators respectively, correspond to the relative phases of each oscillator and indicate that they are approaching an orientational difference of 180°. The positive phase (amplitude) factor assigned to the free OH oscillator (3669 cm$^{-1}$) corresponds to an orientation of the dipole vector on average is pointing toward the aqueous phase or $\theta < 90°$, analogous to that observed for the free OH oscillator of interfacial HOD. Conversely, the negative phase (amplitude) factor attributed to the uncoupled bonded OH oscillator signifies the dipole vector is on average pointing toward the $CCl_4$ phase or $\theta > 90°$.

The fact that both the free and bonded OH spectral features are approaching a phase difference of 180° and considerable VSF intensity is collected under *s,s,p* polarization for both oscillator modes unambiguously indicates that interfacial water molecules generating these two spectral features orient such that they straddle the interface the with bonded OH oscillator directed toward the water phase and the free OH toward the $CCl_4$ phase (Figure 8). The existence of water molecules that straddle the interface is further supported by MD simulations performed at the neat $CCl_4/H_2O$ interface by Chang et al.,[17] and by similar water species observed in the simulation of the $H_2O$/1,2-dichloroethane system. [15] To attain a more quantitative description of the angle either of the OH oscillators makes with the interfacial plane and therefore a precise molecular orientation it is necessary to collect the VSF in-plane response which due to the low signal levels is still in progress.

The third major feature of the neat $CCl_4/H_2O$ interfacial spectrum is the peak at 3247 ± 5 cm$^{-1}$. This peak corresponds to interfacial water molecules that are involved in a tetrahedrally coordinated H-bonding environment. The broad nature of this peak reflects the H-bonding interactions between neighboring water molecules that leads to the delocalized OH stretching vibrations of H-bonded water. The negative phase factor associated with 3247 cm$^{-1}$ feature indicates the molecular dipole orientation is on average pointing toward the $CCl_4$ phase (Figure 8) ($\theta > 90°$, where the angle of $\theta$ is defined as the angle between

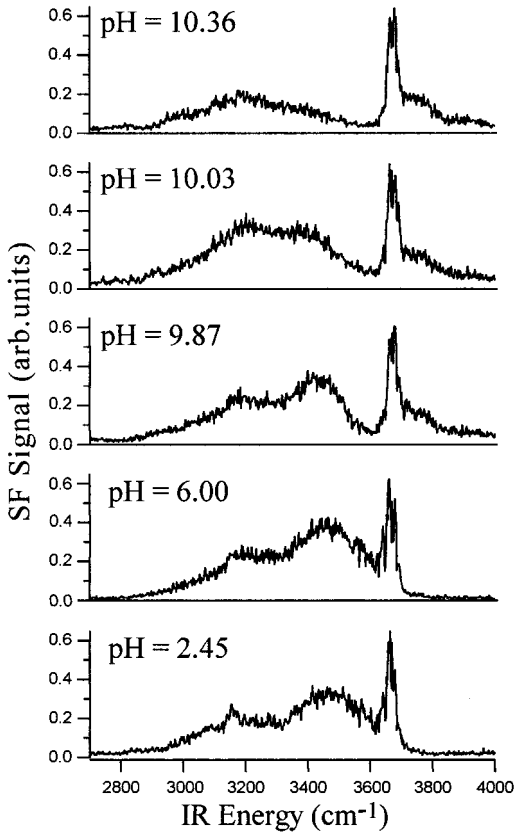


**Figure 7.** VSF spectrum of the neat $CCl_4/H_2O$ interface for a series of pH values. HCl and NaOH solutions were used to adjust the pH of the aqueous phase.

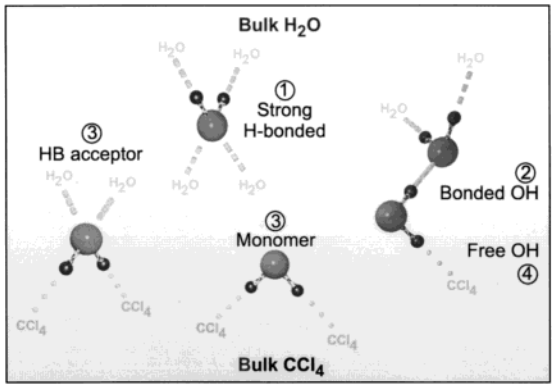


**Figure 8.** Schematic representation of interfacial water species contributing to the VSF spectrum of the neat $CCl_4/H_2O$ interface. Individual water species correspond to the peaks in Figure 6b. Dashed lines represent $H_2O-H_2O$ interactions, and dotted lines represent $H_2O-CCl_4$ interactions.

the symmetry axis of the water molecule and the *Z* axis of the laboratory frame and Z is normal to the interface with 0° pointing directly into the $CCl_4$ phase).

One of the more interesting spectral features of the fitted neat $CCl_4/H_2O$ interfacial spectrum are the OH vibrational bands at $3617 \pm 2$ cm$^{-1}$ and $3716 \pm 3$ cm$^{-1}$, which bracket the localized free OH oscillator feature at 3669 cm$^{-1}$. Their spectral position near the free OH oscillator and narrow bandwidth reflect the minimal H-bond perturbation associated with these modes. Identification of these two modes is based in part upon comparison of these features with the monomeric $\nu_1$ (3616 cm$^{-1}$) and $\nu_3$ (3708 cm$^{-1}$) bands observe in the FTIR studies of monomeric $H_2O$ in bulk $CCl_4$ (Figure 4a) described previously. Thus, we attribute these peaks to either water molecules in the interfacial region that are completely surrounded by $CCl_4$ (monomers) or water molecules that interact with other water molecules solely through electron donor interactions. It can be observed in IR studies of water clusters that water molecules participating in H-bonding solely with the lone electron pairs exhibit very little shift in OH bond frequency. [47,59] OH stretching frequencies are far more sensitive when bonding occurs at the hydrogen atom than at the lone pair of electrons. [47] Water molecules that participate in H-bonding solely with the lone electron pairs are typically labeled a hydrogen bond acceptor (HB acceptor). Because of the limited OH bond perturbation associated with the HB acceptor water molecule, the OH stretching frequencies for such weakly interacting water molecule are found to be similar to those observed for a truly monomeric water species. Within the resolution of these VSF experiments, these two types of water molecules (monomeric and HB acceptor) are spectroscopically indistinguishable. We therefore assign the features at 3617 and 3716 cm$^{-1}$ to the intramolecularly coupled $\nu_1$ and $\nu_3$ modes respectively, of interfacial water molecules that are not participating in H-bonding interactions with their hydrogens. This assignment includes both monomeric and HB acceptor interfacial water molecules.

Although the $\nu_1$ and $\nu_3$ modes of HB acceptor/monomeric water molecules show little sign of H-bonding interactions with other interfacial water molecules they do exhibit an anisotropic orientational distribution, which is reflected by their associated phase (amplitude) factors. Symmetry requires that under $I_{SSP}$ polarization, the $\nu_1$ and $\nu_3$ modes of HB acceptor/monomeric $H_2O$ have opposite phase factors (amplitude sign) meaning they are 180° out of phase. [37] The positive and negative phase factors attributed to the fitted $\nu_1$ (3617 cm$^{-1}$) and $\nu_3$ (3716 cm$^{-1}$) peaks respectively, indicate a molecular orientation such that the molecular dipole vector is on average pointing toward the aqueous phase or $\theta < 90°$ (Figure 8). Bracketing the free OH stretch (3669 cm$^{-1}$), the $\nu_1$ ((+) amplitude) and $\nu_3$ ((−) amplitude) stretching modes will interfere with the dangling OH bond (+ amplitude) due to their close spectral proximity and relative phase differences. The resulting interference produces spectral intensity near 3600 cm$^{-1}$ and very little obvious spectral intensity near 3710 cm$^{-1}$ in the neat $CCl_4/H_2O$ spectrum of Figure 2b. However, the contribution from $\nu_3$ results in the asymmetry on the high energy side of the free OH peak. From the fits to the data and the phase derived from these fits, we conclude that although these are very weakly interacting water molecules, their interaction with the polarizable organic phase causes a net orientation of these molecules with their hydrogens pointed into the $CCl_4$.

It becomes clear that if one considers the nonlinear fit to the neat $CCl_4/H_2O$ VSF spectral data and the series of supporting experiments described above that five (3247, 3439, 3617, 3669, and 3716 cm$^{-1}$) out of six of the fitted peaks encompass the majority of the integrated band intensity for the spectral envelope. The relatively small (0.07 amplitude) peak located at 3570 cm$^{-1}$ makes up the sixth small peak. Although this spectral feature is not significant within experimental error its prevalence in VSF spectroscopic studies of charged surfactants adsorbed at the $CCl_4/H_2O$ interface (to be published) dictates its mention. Its spectral position (3575 cm$^{-1}$) would suggest that these interfacial water molecules are participating in weak H-bonding interactions with surrounding water molecules and therefore might be tentatively assigned to $\nu_1$ of weakly H-bonded water. At this time, a more definite assignment is unjustified, and given that it only makes up 2% of the total integrated band intensity its assignment makes no significant impact on our interpretation or conclusions about the water species present at the $CCl_4/H_2O$ interface.

The interactions between water and the organic phase clearly play an important role in the molecular orientation of water molecules at this interface. To test the interpretation presented above for the neat $CCl_4/H_2O$ interface we have examined the effect of pH on the structure and orientation of water molecules at this interface. Figure 7 displays the VSF spectrum of the neat $CCl_4/H_2O$ interface under various aqueous phase pH conditions. The most distinct changes are observed in the monomeric $\nu_1$ and $\nu_3$ region of the spectrum where water molecules are observed to flip in orientation as the pH is raised. At low (pH = 2.45) to near neutral pH (pH = 6.00), there is very little change in the monomeric/HB acceptor $\nu_1$ and $\nu_3$ region of the VSF spectrum. As the pH is increased, there is a distinct change in the spectrum with a decrease in intensity in the $\nu_1$ region and an increase in the $\nu_3$ region, indicating a change in the average orientation of these monomeric/HB acceptor molecules of ~180°. Such a change in orientation results in the $\nu_1$ mode becoming out-of-phase and the $\nu_3$ mode becoming in-phase with the free OH mode as observed. Although these molecules change their orientation by ~180°, these weakly interacting water molecules continue to show only weak H-bonding character as evidenced by the minimal growth in intensity in either the 3200 or the 3400 $cm^{-1}$ region. VSF studies with various aqueous salt solutions indicate that $Na^+$ and $Cl^-$ counterions play no role in the spectral changes observed herein. We attribute the flip in orientation observed for these interfacial water molecules to a change in interfacial potential caused by the increase in bulk hydroxide ion concentration and possibly the adsorption of hydroxide ions to the interfacial region as observed in previous studies by Marinova et al. [76] The approach or adsorption of a hydroxide ion to the interfacial region can screen $CCl_4-H_2O$ interactions and therefore perturb interfacial water molecules such that they orient with the electric field emanating from the hydroxide ion. Similar effects are observed when a negatively charged surfactant adsorbs at the $CCl_4/H_2O$ interface and will be the focus of a later publication. It is clear however that the presence of hydroxide ions in the interfacial region causes water molecules to behave differently than what is observed for simple salts. Further experiments exploring these effects are in progress.

Figure 8 summarizes and displays a schematic representation of contributing interfacial water species and their average orientation, derived from the nonlinear fit to the neat $CCl_4/H_2O$ VSF data. In summary, water species at the neat $CCl_4/H_2O$ interface include: strongly H-bonded tetrahedrally coordinated $H_2O$ ($\nu_1$(SB)) oriented with hydrogens directed toward aqueous phase, monomeric/HB acceptor $H_2O$ oriented with hydrogens directed toward the $CCl_4$ phase, and intramolecularly uncoupled $H_2O$ that straddles the interface with one proton directed toward the $CCl_4$ phases and the other directed toward the aqueous phase. As previously noted, a more precise description of molecular orientation is still in progress and therefore will be the focus of a later publication.

Although we have described water at the $CCl_4/H_2O$ interface by a static pictorial of water species with specific orientations, the interface is a very dynamic region due to thermal capillary waves which traverse the interface. Therefore, the peaks that we have unequivocally assigned to these various water species are an average over time and represent the most probable molecular configurations of interfacial water molecules in a dynamic environment.

Because the OH oscillator strength of a water molecule can vary significantly with the degree of H-bonding one [1,46,47] must be cautious when quantitatively comparing spectral intensities for each of the spectral features derived from the fit to the data. With this in mind, we can make some general conclusions about the overall structure of water at the $CCl_4/H_2O$ interface. It is clear by inspection of Figure 6b that over half (54%) of the total integrated intensity of the $CCl_4/H_2O$ spectral envelope originates from the uncoupled bonded and free OH oscillator i.e., water molecules which straddle the interface. Given that these two peaks (3669 $cm^{-1}$ & 3439 $cm^{-1}$) originate from the same molecule one can gain insight into the orientation of these interfacial molecules by a comparison of their integrated band intensities. Several groups have identified a linear correlation between the increase in the IR integrated band intensities and the frequency of the OH oscillator of HOD. [47,62] One can ascertain from these IR studies that the band area for a bonded uncoupled OH oscillator (with a peak frequency near 3440 $cm^{-1}$) increases by ~7 times when compared to the free OH oscillator. In our experiments we find that there is only a ~4-fold increase (Figure 6b) in SF band area for the bonded OH stretch (compared to the free OH), which corresponds to $\sqrt{4}$ when comparing it to the IR integrated band areas. One of the most likely explanations for this relatively low difference in intensity between the bonded and unbonded modes of these uncoupled $H_2O$ molecules is that of orientation. This intensity difference is an indication that water molecules which straddle the interface do not lie with their molecular dipole oriented parallel to the interface normal, which would give a ratio of near 14:1 (bonded:free) in VSF experiments, but are oriented such that the free OH points more normal and the bonded OH more parallel to the interfacial plane.

The two peaks corresponding to the $\nu_1$ and $\nu_3$ modes of monomeric/HB acceptor water display relatively little VSF intensity when compared with those that straddle the interface and those that are tetrahedrally coordinated (3247 $cm^{-1}$). There are several possibilities for this: (1) These water molecules are aligned such that they lie nearly parallel to the interface and therefore produce little out of plane response ($I_{s,s,p}$). (2) There are very few of these water species (monomeric/HB acceptor) located in the interfacial region. (3) The integrated band intensities are small due to the lack of H-bonding interaction occurring at the protons. Recent studies performed at the neat $CCl_4/H_2O$ interface under polarization conditions that probe the inplane VSF response ($I_{s,p,s}$) display relatively no intensity in the 3616 $cm^{-1}$ region which suggests that these water molecules are on average oriented such that the hydrogens point into the $CCl_4$ phase. We therefore conclude that the relatively small intensity for these water molecules is due to the fact that there are few of these molecules located in the interfacial region, as you would expect given the limited solubility of $H_2O$ in $CCl_4$. In addition, the OH oscillator is not significantly perturbed by H-bonding interactions which would significantly increase the intensity of this coupled OH stretching mode.

The broad peak observed in this systems at 3247 $cm^{-1}$ represents the most strongly hydrogen bonded water molecules and also represents a broad distribution of interactions in this spectral envelope (284 $cm^{-1}$ fwhm). For comparison, Raman and IR studies of water in its solid form display large prominent spectral bands in the 3100−3200 $cm^{-1}$ with a relatively narrow bandwidth (fwhm < 100 $cm^{-1}$) [1,47−52] These ice spectra have narrow widths and relatively large intensities that suggest that these localized OH oscillators originate from a strong and extended H-bonding network that has extensive intermolecular coupling, possibly a clathrate like structure. [56] In VSF studies of the (0001) surface of ice, this peak is observed at 3150 $cm^{-1}$,[30] significantly red shifted and with a sharper bandwidth than what we observe from our peak corresponding to the strongest hydrogen bonded water. Thus we conclude that the strong hydrogen bonding that has been invoked to explain the vapor/water interface [53,77] is not present at these organic/water

interfaces, but in fact the interfacial water takes on a more disordered nature. The fact that this peak resides in the spectral region (3247 $cm^{-1}$) where liquid water at ambient temperatures is observed [1,47,48,51,52] further supports this assignment. Consistent with this picture is the fact that the uncouple bonded OH oscillator from water molecules that straddle the interface also exhibit a broad spectral distribution (~220 $cm^{-1}$ fwhm) implying weaker and more delocalized H-bonding interactions with neighboring interfacial water. Presumably if the bonded uncoupled OH oscillator were interacting with water molecules which participate in strong H-bonding interactions, like that found in ice, they would exhibit OH oscillator frequencies (near 3275−3375 $cm^{-1}$) similar to those found in IR and Raman spectra of an HOD molecule in an ice lattice or supercooled liquid water. [1,47,48,51,52] Given the fact that all bonded OH stretching modes of water at the $CCl_4/H_2O$ interface exhibit frequencies and bandwidths similar to that of liquid water at room temperature, we can only conclude that H-bonding interactions at the $CCl_4/H_2O$ interface are no stronger that those found in liquid water at room temperature.

It is valuable to compare these results with theoretical efforts in this area. Several theoretical groups have made significant contributions in attaining a molecular level picture of water structure at hydrophobic liquid surfaces by performing molecular dynamics [15,17] and Monte Carlo [18] calculations on several different liquid/liquid interfacial water systems. These simulations examined water adjacent 1,2-dichloroethane, benzene and $CCl_4$, which span a range of molecules having different $H_2O$-organic interactions therefore making a series of simulations to compare with experimental data. Despite the variance in $H_2O$-organic interactions, each of these simulations display very similar results in terms of the water structure and H-bonding environment adjacent the three dissimilar nonpolar phases. Results attained for the liquid/liquid systems are also similar to theoretical models of water at what is considered to be one of the most hydrophobic junctions, the vapor/$H_2O$ interface. [13−15] In short, these simulations conclude that water within the first couple of interfacial layers orient with their dipole parallel to the interfacial plane. Water molecules within the layer nearest the organic phase were found to be oriented such that one hydrogen points into the organic, whereas the other points into the water phase (straddling the interface). These results are similar to our results at the $CCl_4/H_2O$ interface where a large percentage of interfacial water molecules are observed to straddle the interfacial region.

In contrast to simulation results at the benzene/$H_2O$ and 1,2-dichloroethane interfaces, VSF experiments at the $CCl_4/H_2O$ interface display monomeric/HB acceptor water molecules with a significant component of the molecular dipole oriented normal to the interfacial plane such that the protons interact with the organic phase. These molecules largely interact with the organic phase, but remain in the interfacial region as evidenced by their orientational nature. (Those that are randomly oriented should not appear in the SF spectrum.) Although the $CCl_4/H_2O$ simulation accurately predicted water molecules oriented such that both hydrogens interact with the organic phase (HB acceptor), a single oriented water molecule that fully penetrated into the organic phase or was completely surrounded by the organic molecules (monomeric) was absent from each of the liquid/liquid simulations. The spectral fittings and phase information derived do not unequivocally demonstrate the existence of interfacial water that have fully penetrated the organic phase but combined with pH experiments presented above and a series of charged surfactant studies at the $CCl_4/H_2O$ interface (to be published) are evidence in favor of monomeric water species at the $CCl_4/H_2O$ interface. VSF experiments at various alkane/$H_2O$ interfaces also show similar monomeric and/or HB acceptor water molecules.

Each of the liquid/liquid simulations also support the idea that as water molecules approach the interfacial region each water molecule becomes *more strongly hydrogen bonded* to fewer water molecules, similar to that observed at the vapor/$H_2O$ interface. [15] This would imply that the spectroscopy of interfacial water at both organic/$H_2O$ and vapor/$H_2O$ interfaces will reflect similar strong H-bonding environments which it does not. It is interesting to compare these studies with those of a statistical mechanics approach to understanding water at solid hydrophobic surfaces. These theoretical studies support the idea that hydrophobic hydration of surfaces of nanometer dimensions induce a low-density region (vapor phase or drying of the surface) of water leading to the strong attraction between large hydrophobic objects. This hydrophobic attraction is a result of the disruption of H-bonds at the surface. Although these VSF studies do indicate a disruption of hydrogen bonding at the organic/water interface relative to bulk water, the spectra do not exhibit specific spectral features attributable to a "vapor" drying layer adjacent to the hydrophobic liquid, as would be manifested in spectral features of isolated gas phase water molecules. These studies do not preclude the existence of a low-density region of water molecules or a low-density region of a mixture of $CCl_4$ and $H_2O$. However, this region would need to be relatively limited in dimension to cause the kind of orientation of these interfacial molecules, both the ones that straddle the two phases and those that are directed with their hydrogens toward the $CCl_4$ phase, that is observed here.

## Summary and Conclusions

The hydrophobic effect and the hydration of hydrophobic macromolecules and surfaces continues to intrigue scientists across the disciplines because of the key role that these issues play in technology, biology, and the environment. The paper presents insight into the nature of the hydration of hydrophobic planar liquids. In particular, the studies show that in contrast to models describing the hydrophobic effect where a small nonpolar solute in water tends to enhance water hydrogen bonding in its vicinity, water at a planar hydrophobic surface has weaker hydrogen bonding interactions with other water molecules than occurs in the bulk phase. This weakening is manifested in a dominance of spectral intensity in the region where water molecules show minimal interaction with other water molecules. Accompanying the weakening of the $H_2O$−$H_2O$ interactions is the increased importance of $CCl_4$−$H_2O$ and hydrocarbon-$H_2O$ interactions. Such interactions are strong enough to result in significant orientation of water molecules that either straddle the interface or orient into the organic phase. The existence of these organic-water interactions, whereas not explicitly addressed in most theoretical models of water/hydrophobic interfaces, is manifested in our everyday experience. A small drop of insoluble oil on a water surface will spread to form a monolayer on that surface. Additional evidence is provided by the stability of thin films of water on hydrophobic surfaces, the basis behind mineral flotation. The results presented here are also consistent with the difference in the thermodynamics of the hydration of a small nonpolar solute and the hydration of a large hydrophobic surface. From a free energy perspective, both cases are unfavorable. [19] However, the entropy and enthalpy terms act in very different ways. As the molecular dimension of the hydrated species increases, the system can no longer be in a regime where water can continue to hydrogen bond to neighboring water molecules as it did in the presence of a small solute. Hence, the entropy term for the solute is negative whereas for the large hydrophobe or surface, it is positive. For a

hydrocarbon surface, the interfacial energy, or free energy needed to create the interface, decreases with temperature because of the increasing importance of the positive entropy term. For the nonpolar solute, the free energy of transfer decreases with temperature because of the negative entropy term. From a fundamental perspective, the outstanding question is one of dimension; what molecular scale is appropriate for these two different effects and what happens at intermediate length scales? [16,20,22]

For those interested in applying the results presented in this paper to issues of the role of water in creating three-dimensional structures, particularly for application to protein folding and macromolecular assembly, it is clear that the molecular polarizability of the hydrophobic phase must be taken into account in any model. This interaction results in the kind of attractive and orienting interactions observed here between highly polar OH bonds and the hydrocarbon or $CCl_4$ molecules. Because proteins and most macromolecular assemblies also contain charged species, such additional interactive species must be taken into account when thinking about how water structures near a hydrophobic surface. This will be the topic of an upcoming paper where the structure of water around small charges embedded at the organic/water interface has been investigated. [78]

**Acknowledgment.** We gratefully acknowledge the financial assistance of the National Science Foundation, CHE-9725751, for support of the liquid/liquid portion of these studies and the Department of Energy, Basic Energy Sciences for the air/water studies. Input from Dr. Mac Brown and Betsy Raymond are also appreciated and acknowledged.

## References and Notes

(1) Eisenberg, D.; Kauzmann, W. *The Structure and Properties of Water*; Oxford University Press: New York, 1969.
(2) Silverstein, T. P. *J. Chem. Educ.* **1998**, *75*, 116−118.
(3) Pratt, L. R.; Chandler, D. *J. Chem. Phys.* **1977**, *67*, 3683−3704.
(4) Geiger, A.; Rahaman, A.; Stillinger, F. H. *J. Chem. Phys.* **1979**, *70*, 263.
(5) Swaminathan, S.; Harrison, S. W.; Beveridge, D. L. *J. Am. Chem. Soc.* **1978**, *100*, 5705.
(6) Rossky, P. J.; Karplus, M. *J. Am. Chem. Soc.* **1979**, *101*, 1913.
(7) Pollack, G. L. *Science* **1991**, *251*, 1323.
(8) Blokzijl, W.; Engberts, J. B. F. N. *Angew. Chem., Int. Ed. Engl.* **1993**, *32*, 1545−1597.
(9) Frank, H. S.; Evans, M. W. *J. Chem. Phys.* **1945**, *13*, 507.
(10) Wiggins, P. M. *Physica A* **1997**, *238*, 113−128.
(11) Chothia, C.; Janin, J. *Nature* **1975**, *256*, 705−708.
(12) Robinson, G. W.; Cho, C. H. *Biophys. J.* **1999**, *77*, 3311−3318.
(13) Townsend, R. M.; Rice, S. A. *J. Chem. Phys.* **1991**, *94*, 2207.
(14) Wilson, M. A.; Pohorille, A.; Pratt, L. R. *J. Phys. Chem.* **1987**, *91*, 4873−4878.
(15) Benjamin, I. *J. Chem. Phys.* **1992**, *97*, 1432−1445.
(16) Lee, C. Y.; McCammon, J. A.; Rossky, P. J. *J. Chem. Phys.* **1984**, *80*, 4448.
(17) Chang, T.; Dang, L. X. *J. Chem. Phys.* **1996**, *104*, 6772−6783.
(18) Linse, P. *J. Chem. Phys.* **1987**, *86*, 4177−4187.
(19) Schrader, M. E.; Loeb, G. I. *Modern Approaches to Wettability*; Plenum Press: New York, 1992.
(20) Hummer, G.; Garde, S.; García, A. E.; Paulaitis, M. E.; Pratt, L. R. *J. Phys. Chem. B* **1998**, *102*, 10 469−10 482.
(21) Hummer, G.; Garde, S.; Garcia, A. E.; Pratt, L. R. *Chem. Phys.* **2000**, *258*, 349−370.
(22) Lum, K.; Chandler, D.; Weeks, J. D. *J. Phys. Chem. B* **1999**, *103*, 4570−4577.
(23) Stillinger, F. H. *J. Soln. Chem.* **1973**, *2*, 141 158
(24) Yeganeh, M. S.; Dougal, S. M.; Pink, H. S. *Phys. Rev. Lett.* **1999**, *83*, 1179−1182.
(25) Bain, C. D. *J. Chem. Soc., Faraday Trans.* **1995**, *91*, 1281−1296.
(26) Shen, Y. R. *Nature* **1989**, *337*, 519.
(27) Du, Q.; Freysz, E.; Shen, Y. R. *Science* **1994**, *264*, 826−8.
(28) Baldelli, S.; Schnitzer, C.; Shultz, M. J.; Campbell, D. J. *J. Phys. Chem. B* **1997**, *101*, 10 435−10 441.
(29) Gragson, D. E.; Richmond, G. L. *J. Am. Chem. Soc.* **1998**, *120*, 366−375.
(30) Wei, X.; Miranda, B.; Shen, Y. R. *Phys. Rev. Lett.* **2001**, *86*, 1554−1557.
(31) Richmond, G. L. *Annu. Rev. Phys. Chem.* **2001**, *52*, 357−389.
(32) Du, Q.; Freysz, E.; Shen, Y. R. *Phys. Rev. Lett.* **1994**, *72*, 238−41.
(33) Shen, Y. R. *The Principles of Nonlinear Optics*; 1st ed.; John Wiley & Sons: New York, 1984.
(34) Hirose, C.; Akamatsu, N.; Domen, K. *Appl. Spectrosc.* **1992**, *46*, 1051−1072.
(35) Lobau, J.; Wolfrum, K. *J Opt. Soc. Am. B* **1997**, *14*, 2505−2512.
(36) Gragson, D. E.; McCarty, B. M.; Richmond, G. L. *J. Phys. Chem.* **1996**, *100*, 14 272−14 275.
(37) Brown, M. G.; Raymond, E. A.; Allen, H. C.; Scatena, L. F.; Richmond, G. L. *J. Phys. Chem* **2000**, *104*, 10 220−10 226.
(38) Wolfrum, K.; Laubereau, A. *Chem. Phys. Lett.* **1994**, *228*, 83−88.
(39) Conboy, J. C.; Messmer, M. C.; Richmond, G. L. *J. Phys. Chem.* **1996**, *100*, 7617−22.
(40) Bloembergen, N.; Pershan, P. S. *Phys. Rev.* **1962**, *128*, 606−622.
(41) Dick, B.; Gierulski, A. *Appl. Phys. B* **1985**, *38*, 107−116.
(42) Gragson, D. E.; Alavi, D. S.; Richmond, G. L. *Opt. Lett.* **1995**, *20*, 1991.
(43) Gragson, D. E.; McCarty, B. M.; Richmond, G. L.; Alavi, D. S. *J. Opt. Soc. Am. B* **1996**, *13*.
(44) Scatena, L. F.; Brown, M. G.; Richmond, G. L. *Science* **2001**, *292*, 908−912.
(45) Brown, M. G.; Walker, D. S.; Richmond, G. L., in preparation.
(46) Jeffrey, G. A. *An Introduction to Hydrogen Bonding*; Oxford University Press: New York, 1997.
(47) Scherer, J. R. The *Vibrational Spectroscopy of Water*; Clark, R. J. H. and Hester, R. E., Eds.; Heyden: Philadelphia, 1978; Vol. 5, pp 149−216.
(48) Scherer, J. R.; Snyder, R. G. *J. Chem. Phys.* **1977**, *67*, 794.
(49) Scherer, J. R.; Go, M. K.; Kint, S. *J. Phys. Chem.* **1974**, *78*, 1304−1313.
(50) Rice, S. A. *Structure of Liquids*; Springer-Verlag: New York, 1975; Vol. 60.
(51) Green, J. L.; Lacey, A. R.; Sceats, M. G. *J. Phys. Chem.* **1986**, *90*, 3958.
(52) Hare, D. E.; Sorensen, C. M. *J. Chem. Phys.* **1992**, *96*, 13.
(53) Du, Q.; Superfine, R.; Freysz, E.; Shen, Y. R. *Phys. Rev. Lett.* **1993**, *70*, 2313−16.
(54) Yalamanchili, M. R.; Atia, A. A.; Miller, J. D. *Langmuir* **1996**, *12*, 4176−4184.
(55) Whalley, E. *Can. J. Chem.* **1977**, *55*, 3492−3441.
(56) Walrafen, G. E.; Yang, W. H.; Chu, Y. C. *ACS Symp. Ser.* **1997**, *676*, 287.
(57) Allen, H. C.; Raymond, E. A.; Richmond, G. L. *J. Phys. Chem. A* **2001**, *105*, 1649−1655.
(58) Reimers, J. R.; Watts, R. O. *Chem. Phys.* **1984**, *85*, 83−112.
(59) Huang, Z. S.; Miller, R. E. *J. Chem. Phys.* **1989**, *91*, 6613−6631.
(60) Gragson, D. E.; Richmond, G. L. *Langmuir* **1997**, *13*, 4804−4806.
(61) Downey, J. R. J.; Choppin, G. R. *Spectrochim. Acta* **1974**, *30 A*, 37−42.
(62) Glew, D. N.; Rath, N. S. *Can. J. Chem.* **1971**, *49*, 837−56.
(63) Luck, W. A. P.; Klein, D.; Rangsriwatananon, K. *J. Mol. Struct.* **1997**, *416*, 287−296.
(64) Zoidis, E.; Yarwood, J.; Tassaing, T.; Danten, Y.; Besnard, M. *J. Mol. Liq.* **1995**, *64*, 197−210.
(65) Gragson, D. E.; Richmond, G. L. *J. Phys. Chem. B* **1998**, *102*, 3847−3861.
(66) Green, J. L.; Lacey, A. R.; Sceats, M. G. *Chem. Phys. Lett.* **1986**, *130*, 67−71.
(67) Wall, T. T.; Hornig, D. F. *J. Chem. Phys.* **1965**, *43*, 2079−2087.
(68) Devlin, J. P. *J. Chem. Phys.* **1989**, *90*, 1322−1329.
(69) Kint, S.; Scherer, J. R. *J. Chem. Phys.* **1978**, *69*, 1429−1431.
(70) Gragson, D. E.; Richmond, G. L. *J. Phys. Chem. B* **1998**, *102*, 569−576.
(71) Raymond, E. A.; Tarbuck, T.; Richmond, G. L. (in preparation).
(72) Danten, Y.; Tassaing, T.; Besnard, M. *J. Phys. Chem. A* **2000**, *104*, 9415−9427.
(73) Choppin, G. R.; Downey, J. R. Jr. *J. Chem. Phys.* **1972**, *56*, 5899−5903.
(74) Conrad, M. P.; Strauss, H. L. *J. Phys. Chem.* **1987**, *91*, 1668−1673.
(75) Waldron, R. D. *J. Chem. Phys.* **1957**, *26*, 809−814.
(76) Marinova, K. G.; Alargova, R. G.; Denkov, N. D.; Velev, O. D.; Petsev, I. B.; Ivonova, I. B.; Borwankar, R. P. *Langmuir* **1995**, *12*, 2045−2051.
(77) Wei, X.; Shen, Y. R. *Phys. Rev. Lett.* **2001**, *86*, 4799−4802.
(78) Scatena, L. F.; Richmond, G. L. (in preparation).